Title: **Extraction of Protein Dynamics Information Hidden in Cryo-EM Map Using Deep Learning**

Author: Shigeyuki Matsumoto[1,*], Shoichi Ishida[2,*], Mitsugu Araki[3], Takayuki Kato[5], Kei Terayama[1,3,6,†], Yasushi Okuno[1,3,†]

Author information

These authors contributed equally: Shigeyuki Matsumoto, Shoichi Ishida

Affiliations

[1] Medical Sciences Innovation Hub Program, RIKEN Cluster for Science, Technology and innovation Hub, Tsurumi-ku, Kanagawa, Japan

[2] Graduate School of Pharmaceutical Sciences, Kyoto University, Yoshida, Sakyo-ku, 606-8501 Kyoto, Japan

[3] Graduate School of Medicine, Kyoto University, 53 Shogoin-Kawaharacho, Sakyo-ku, 606-8507, Kyoto, Japan

[4] Research and Development Group for In Silico Drug Discovery, Center for Cluster Development and Coordination (CCD), Foundation for Biomedical Research and Innovation at Kobe (FBRI) 6-3-5, Minatojima-Minamimachi Chuo-ku, Kobe Japan, Hyogo, Japan

[5] Institute for Protein Research, Osaka University, Suita, 565-0871 Osaka, Japan.

[6] RIKEN Center for Advanced Intelligence Project, Nihonbashi, Tokyo 103-0027, Japan.

Author contributions

S.M., S.I., K.T., and Y.O. designed the study. S.M., and S.I. performed pre-processing of cryo-EM map, construction of neural networks, model trainings and analyses in DEFMap. S.M. and M.A. performed MD calculations. S.M. and T.K. performed preparation of original cryo-EM map data. K.T. and Y.O. conceived the idea for the project. S.M. and S.I. wrote the manuscript. All the authors discussed, edited the manuscript, and approved the final version of the manuscript.

Corresponding authors

Correspondence to Kei Terayama (kei.terayama@riken.jp) and Yasushi Okuno (okuno.yasushi.4c@kyoto-u.ac.jp).

Abstract

Protein functions are associated with their three-dimensional structures and in-solution dynamics. After the technical breakthroughs in cryogenic electron microscopy (cryo-EM) single-particle analysis (SPA), numerous structures have been solved at atomic ~ near-atomic resolutions, including extremely large macromolecules that were not solved by conventional techniques. Their dynamics analysis based on the solved structures further deepens the understandings of the functional mechanisms. However, the elucidations are often hampered by the large molecular sizes and the complicated structural assemblies making both the experimental and computational approaches challenging. Here, we report a deep learning-based approach, DEFMap, to extract the dynamics information "hidden" in a given cryo-EM density map, using a three-dimensional convolutional neural network (3D-CNN). DEFMap successfully provided dynamics information equivalent to molecular dynamics (MD) simulation and experimental approaches only from cryo-EM maps. Indeed, DEFMap has detected dynamics changes associated with molecular recognitions and the accompanying allosteric conformational stabilizations. We expect that this new approach allows cryo-EM SPA to quantitatively grasp the in-solution protein behavior at atomic and residue levels beyond the static information, gaining biological insights into the functional mechanisms.

Main

Protein functions under physiological conditions are associated with the three-dimensional structures and in-solution dynamics. Therefore, their investigations at high resolutions are essential for elucidations of the molecular mechanisms underlying biological events, such as regulations in cellular signaling mediated by protein-protein interaction and metabolisms catalyzed by enzymes[1,2]. To determine the protein structures, various structural biology techniques, such as nuclear magnetic resonance (NMR), X-ray crystallography, and cryo-EM SPA[3-5], have been developed over the decades[6]. Along with their techniques, the dynamics information has been quantitatively measured through several experimental and computational approaches, such as NMR, hydrogen-deuterium exchange (HDX) mass spectroscopy (MS)[7], and MD simulations[8].

Recent breakthroughs in cryo-EM SPA have uncovered numerous structures of biological molecules at atomic or near-atomic resolutions, including extremely large macromolecules that have not been solved by conventional techniques. However, the dynamics investigations of the molecules targeted in cryo-EM studies are technically

challenging in both experimental and computational approaches due to the large molecular sizes and the complicated structural assemblies.

Here, we report a deep-learning-based approach to investigate dynamics information using only a cryo-EM map. Three-dimensional cryo-EM maps solved by SPA are reconstructed from a vast number of two-dimensional molecular particle images in the micrographs[3-5]. In the cryo-EM SPA, the specimens are prepared by rapidly freezing the macromolecule solutions in which proteins adopt variable conformations. Therefore, the dynamics properties are "hidden" in the reconstructed cryo-EM maps. In this regard, an approach, manifold embedding, was reported to investigate the conformational heterogeneity using the two-dimensional particle images[9]. Nevertheless, avenues for the direct extraction of the dynamics information only from the cryo-EM maps have not been challenged, while researchers have known that the local map intensities are, to some extent, correlated with the dynamic properties, i.e., the intensities at flexible regions are weakened.

Our approach aims to quantitatively extract the hidden dynamics information at atomic or residue levels only from distributions of density data in cryo-EM maps, named as DEFMap (Dynamics Extraction From cryo-em Map). DEFMap determines the dynamics corresponding to root-mean-square fluctuation (RMSF) values representing atomic fluctuations around the average structure in MD simulations. We utilized one of the deep-learning methods, 3D-CNN[10-12], which is widely used to detect or classify three-dimensional objects constructed from several resources, such as a video data[12-14] and magnetic resonance imaging[15-17]. Moreover, 3D-CNN has been shown to exhibit remarkable performance on the three-dimensional cryo-EM maps to recognize several structural patterns, such as secondary structures, amino acids, and the local map resolutions[18-21].

DEFMap has a neural network architecture consisting of 3D convolutional blocks and dense blocks (Fig. 1a). DEFMap reads 15^3 $Å^3$ sub-voxels generated from low-pass filtered cryo-EM maps and assigns the logarithmic RMSF of the heavy atoms to each grid based on the density data. We defined residue-specific values as residue-averages of normalized outputs from DEFMap and used them for the following evaluations and analyses (see post-processing and visualization of output from a neural network in Methods). Hereafter, the residue-specific values of DEFMap- and MD-derived dynamics are termed as $\text{Dynamics}^{\text{DEFMap}}$ and $\text{Dynamics}^{\text{MD}}$, respectively.

We collected twenty-five cryo-EM maps with the overall resolution of less than 4.5 Å from Protein Data Bank (PDB)[22,23] as training dataset (Supplementary Table 1, average overall resolution = 3.62 $\pm$ 0.46) and their hidden dynamics were derived from MD

simulations using the corresponding atomic models as initial structures (see molecular dynamics simulations in Methods). Within the training dataset, the map intensities tended to correlate with the $Dynamics^{MD}$ as generally considered but appears to be insufficient for the direct estimations of the dynamics since the correlation coefficient values (r) were not good as 0.464 ± 0.164 (Fig. 1b left and Supplementary Table 2).

Using the same dataset and the dynamics data, we employed leave-one-out cross-validation to evaluate the performance of DEFMap for each protein. The result showed that the correlations were globally improved to allow for inference of the dynamics equivalent to $Dynamics^{MD}$ ($r = 0.665 \pm 0.124$), indicating that DEFMap efficiently extracts the features representing dynamics from the spatially configured cryo-EM maps through 3D CNN (Fig. 1b right and Supplementary Table 2).

Subsequently, DEFMap was trained by all data available in the training dataset (twenty-five cryo-EM maps), and in turn, was applied to additional three cryo-EM maps (EMD-4241[24], EMD-7113[25], and EMD-20308[26]) for further evaluation of the DEFMap potential to the structural analyses (Supplementary Table 1). The overview of DEFMap-based dynamics extractions was shown in Figure 2. The dynamics values calculated by the trained model showed good correlation with those derived from MD at both atomic levels (r = 0.704, 0.726 and 0.673, respectively) and residue levels (r = 0.727, 0.748 and 0.711, respectively) (Supplementary Fig. 1). The results indicated that DEFMap correctly extracts dynamics information only from the cryo-EM map data. The mappings of $Dynamics^{DEFMap}$ onto the corresponding atomic models (PDB entry 6FE8, 6BLY, and 6PCV, respectively) demonstrated that DEFMap captured the conformational aspects, such as rigidities at the protein interiors and the flexibilities of the solvent-exposed secondary structure elements, as well as $Dynamics^{MD}$ (Fig. 2a-c, upper panels). The relative dynamics properties in $Dynamics^{DEFMap}$ were well-agreed throughout the molecules with those found in $Dynamics^{MD}$ as represented in their overall profiles (Fig. 2a-c, lower panels). For some regions, the DEFMap-based dynamics extractions were relatively failed. We envisaged that the lower local map resolutions would hinder the accurate extractions. Indeed, the lower the overall map resolution is, especially over 8 Å, the performances were hampered (Fig. 2d and Supplementary Figure 2). This tendency is plausible since the detailed structural information was lost in low-resolution maps. We think that the resolution dependency of the model implies a possibility to further improve the DEFMap performance in the near future since the resolutions are improving year by year through developments of equipment for cryo-EM data acquisition, such as a cold field emission gun.

The consistency with the experimentally derived dynamics should reinforce the potential of DEFMap. Under appropriate conditions, the dynamics of such large proteins targeted by cryo-EM can be experimentally determined by HDX-MS[7], in which the dynamics information is obtained at peptide fragment levels by monitoring deuterium incorporation into protein amide groups (Supplementary Figure 3). Among the above three test proteins, a series of HDX-MS data are available for EMD-20308[26]. $\text{Dynamics}^{\text{DEFMap}}$ averaged for each fragment detected in the referred experiments were well correlated with the corresponding HDX rate (r = 0.743) as well as those for $\text{Dynamics}^{\text{MD}}$ (r = 0.791), supporting that DEFMap actually captured the local dynamics and thus would provide an insight equivalent to experiment-derived one without additional experiments (Fig. 3).

Finally, we explored the potential of DEFMap into biological studies, such as identifications of molecular binding sites and the allosteric effects triggered by ligand bindings, through dynamics extractions based on ligand-induced perturbations of the cryo-EM maps. Ligand-bindings are fundamental biological events and are often accompanied with suppressions of dynamics at the recognition interfaces. Accordingly, we tried to detect the ligand-induced dynamics changes with DEFMap for three pairs of apo/holo proteins unused in the training dataset (apo, holo; EMD-20080, EMD-20081[27]; EMD-9616, EMD-9622[28]; EMD-3957, EMD-3956[29]) (Supplementary Table 1). The overall profiles of $\text{Dynamics}^{\text{DEFMap}}$ were agreed with those of $\text{Dynamics}^{\text{MD}}$ as well as in the above cases (Supplementary Figure 4). Moreover, the dynamics of the residues located nearby the binding partners were significantly suppressed by the ligand bindings (Fig. 4a, b and Supplementary Table 3), demonstrating that the conformational stabilizations at the binding interfaces were detected with DEFMap. Among the residues located at the interfaces (Supplementary Table 3), prominent dynamics suppressions were observed for the regions intensively discussed in the referred literature[27-29], suggesting that the key interactions in the complex formation were identified from the density data (Fig. 4b). Intriguingly, the additional dynamics suppressions were found at the regions distal from the ligand-binding site in EMD-20080/EMD-20081[27] (Fig. 4c). These observations indicated that the ligand-binding allosterically stabilized their regions. In the static models constructed from the cryo-EM maps, no substantial differences were observed for their regions between the apo and holo proteins (Supplementary Figure 5). This observation emphasized the potential of DEFMap to provide dynamics information not accessible from static tertiary structures.

Cryo-EM SPA opened a new era in molecular biology through solving three-dimensional structures of macromolecules and supra-molecules. The complementary use

of DEFMap with the conventional cryo-EM SPA would accelerate the elucidations of the molecular mechanisms underlying the biological events. It is noteworthy that DEFMap requires only cryo-EM maps as inputs, being applicable to macromolecules with extremely large molecular sizes and the complicated structural assemblies, which make the dynamics investigations through conventional MD simulations and experimental techniques difficult in principle. Moreover, any researchers can access the dynamic properties without additional experiments requiring costs, time-consumptions, and in-deep expertise. The present study showed the advanced usage of the structural data derived from cryo-EM SPA and the potential of the deep learning-based techniques in structural biology studies. We believe that DEFMap will be one of the promising choices in the data-driven structural investigations to clarify protein functions.

Figure legends

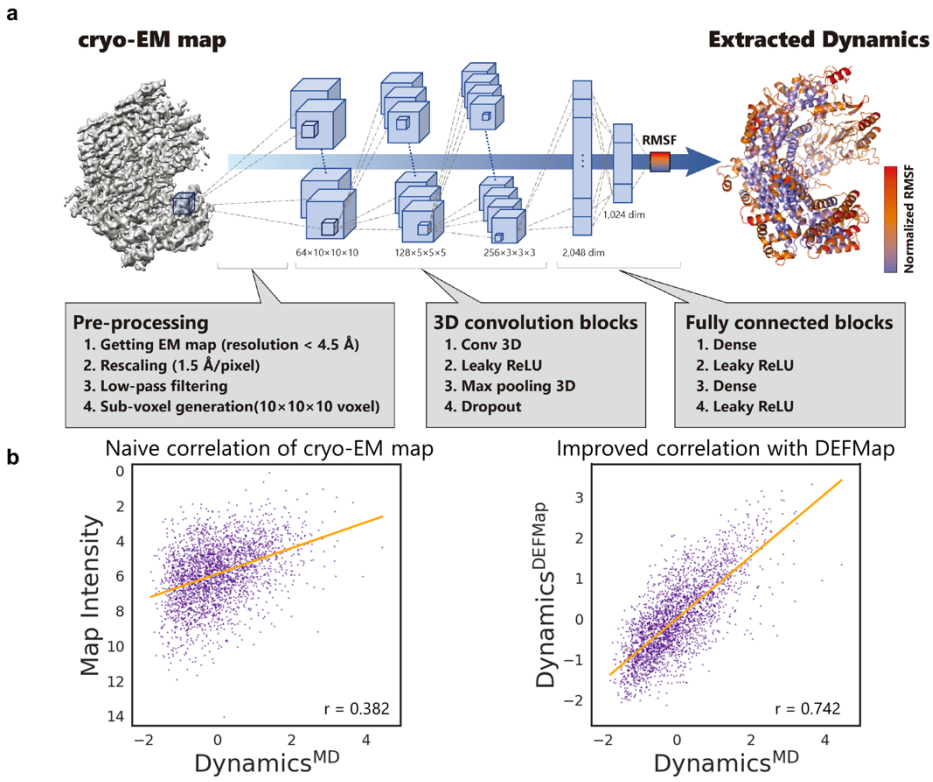

Fig 1: DEFMap-based extraction of dynamics from cryo-EM map. (**a**) Workflow of DEFMap. The Architecture of DEFMap consists of three parts: pre-processing, neural networks, and dynamics visualization after post-processing. In the pre-processing part, sub-voxels (10×10×10 voxel) are generated from an original cryo-EM map with low-pass filtering and rescaling of the grid length as 1.5 Å/pixel. In the neural network part, each generated voxel is converted to the dynamics value representing logarithmic RMSF value using 3D-CNN and fully connected neural networks. In the dynamics visualization part, the calculated dynamics values are averaged for each residue after normalizations and mapped onto the corresponding atomic models. The color bar represents a logarithmic normalized RMSF value. (**b**) Correlation plots of cryo-EM map intensity (left) and $\text{Dynamics}^{\text{DEFMap}}$ (right) against $\text{Dynamics}^{\text{MD}}$. The representative correlation plots in leave-one-out cross-validation (Fold 1 in Supplementary Table 2) are shown. Each point and the regression lines are colored purple and orange, respectively. *r* denotes the correlation coefficient value.

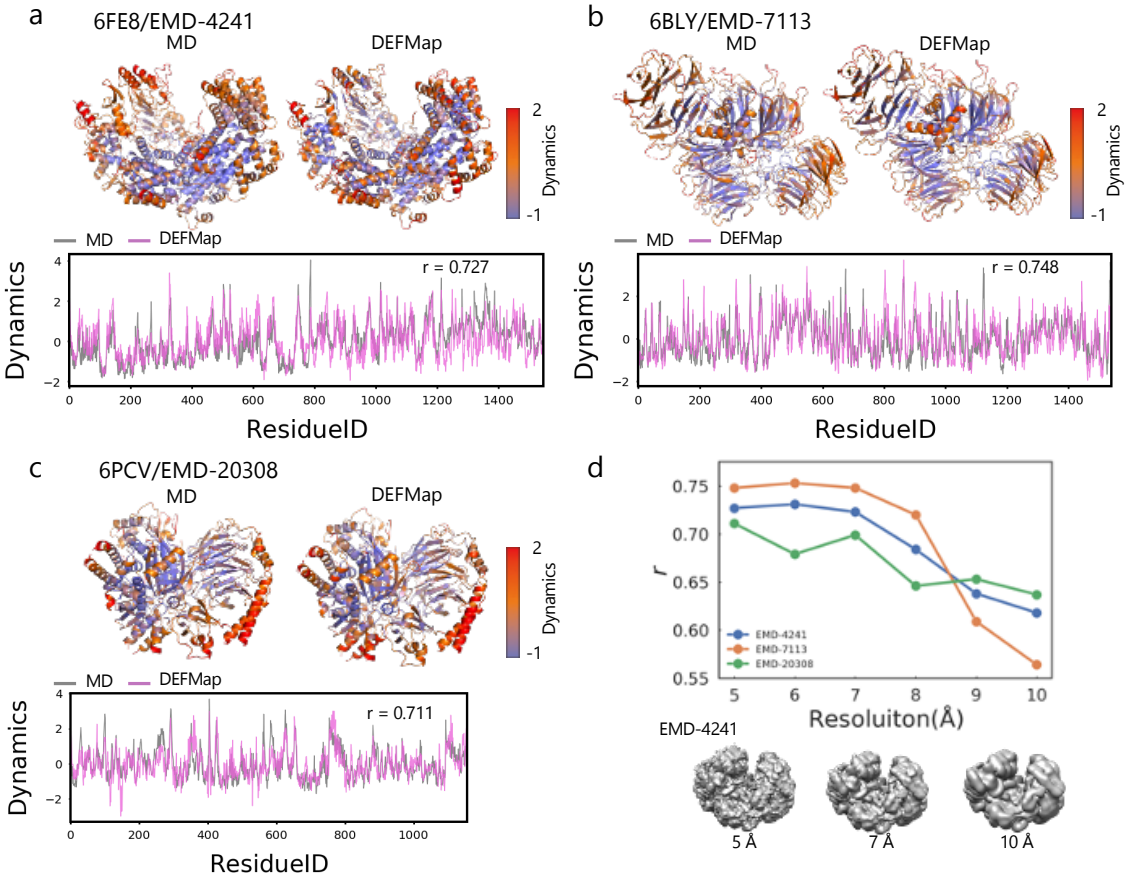

Fig 2: Performance of DEFMap against proteins in the evaluation dataset and its visualization. Dynamics^{MD} and Dynamics^{DEFMap} for 6FE8/EMD-4241 (**a**), 6BLY/EMD-7113 (**b**) and 6PCV/EMD-20308 (**c**). The cryo-EM maps of the training and evaluation datasets were pre-processed by 5.0 Å low-pass filter using the program EMAN2[30]. The residue-specific dynamics values are calculated by averaging the normalized atomic dynamics for each residue. Their values are mapped onto the three-dimensional atomic models (upper panels) by a gradual color change, from blue (-1) to red (2). The color bar represents the dynamics value. The mapping structures with Dynamics^{MD} and Dynamics^{DEFMap} are shown left-hand and right-hand sides, respectively, in each panel. The residue IDs in the overall dynamics profiles (lower panels) are numbered according to the residue orders emerging in the given PDB files. In the profiles, Dynamics^{MD} and Dynamics^{DEFMap} are indicated by gray and pink lines, respectively, and *r* denotes the correlation coefficient value between Dynamics^{MD} and Dynamics^{DEFMap}. **d**, Map resolution-dependency for the dynamics-extraction performance. The correlation coefficient values (*r*) between Dynamics^{MD} and Dynamics^{DEFMap} at the indicated resolutions are plotted. The maps of the training and evaluation datasets were pre-processed to be identical resolutions with low-pass filters (e.g. dynamics extraction from

10.0 Å low-pass filtered test map was carried out with the model trained by the 10.0 Å maps). The values for EMD-4241, EMD-7113, and EMD-20308 are indicated by blue, orange and green lines, respectively. The low-pass filtered maps of EMD-4241 at 5.0 Å, 7.0 Å, and 10.0 Å are shown at bottom.

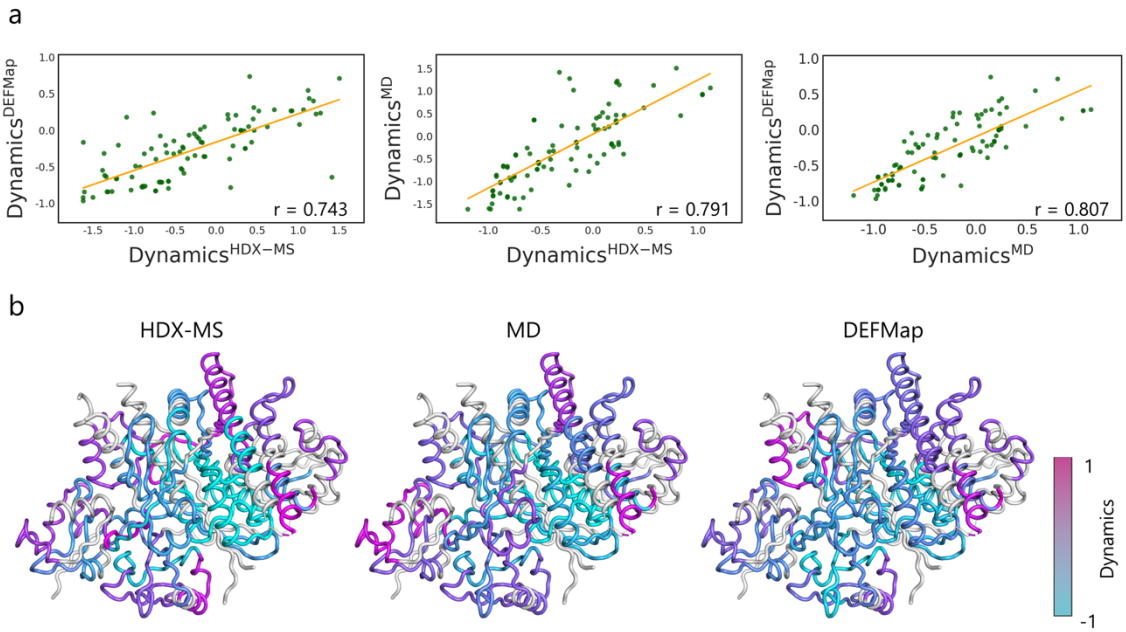

Fig 3: Correspondence between DEFMap-calculated and experimentally derived dynamics. a, Correlation plot of dynamics derived from DEFMap against those determined by HDX-MS. The HDX rates at 10,000 sec for Rac exchanger 1 complexed with G protein beta gamma subunits[26] are normalized within the detected fragments and used as experimentally derived dynamics. The residue-specifics dynamics obtained from MD and DEFMap are converted to fragment-specific values by averaging them for each fragment in the atomic model. The correlation plots between HDX-MS and DEFMap (r = 0.743), HDX-MS and MD (r = 0.807), and MD and HDX-MS (r = 0.791) are shown in left, middle, and right panels, respectively, along with their regression lines (orange). **b**, Spatial distribution of the fragment-specific dynamics on the atomic model. The dynamics values for the representative fragments are mapped onto the atomic model by a gradual color change, from cyan (-1) to magenta (1) (HDX-MS, left; MD, middle; DEFMap, right). The color bar represents the dynamics value at a fragment level. The fragments not detected in the HDX-MS experiments are colored gray.

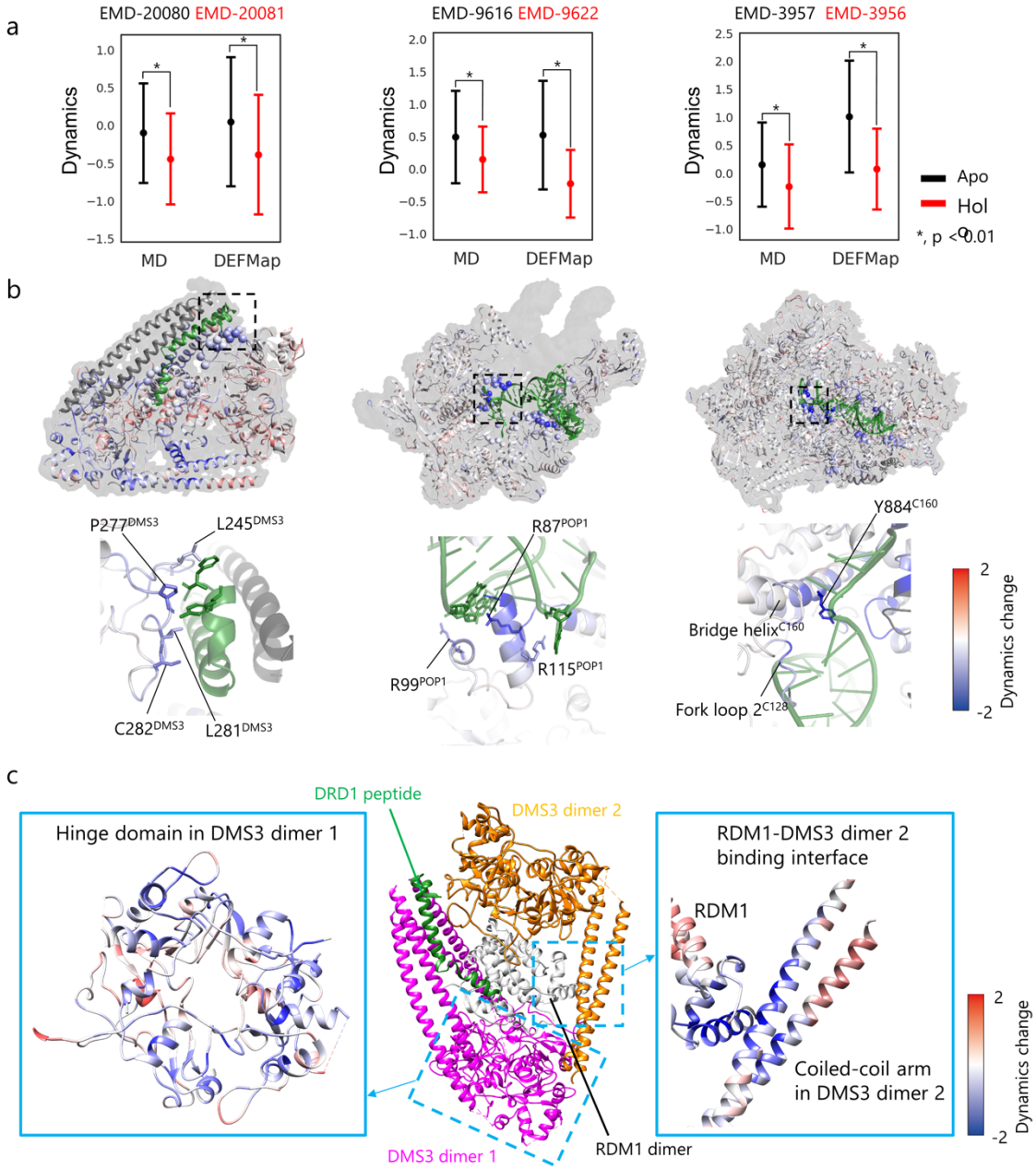

Fig 4: Detection of dynamics alterations induced by ligand bindings. a, Ligand-induced dynamics suppressions at the binding interfaces. The dynamics extractions were carried out using the 5 Å low-pass filtered cryo-EM maps. The dynamics at the binding interfaces in apo (black) and holo (red) proteins are calculated by averaging $\text{Dynamics}^{\text{MD}}$ and $\text{Dynamics}^{\text{DEFMap}}$ for the residues located within 5 Å of the binding partners, and their standard deviations are indicated by error bars (*, $p < 0.01$). **b**, Spatial distributions of the ligand-induced dynamics changes derived from DEFMap. The dynamics changes, which are calculated by subtracting $\text{Dynamics}^{\text{DEFMap}}$ in apo proteins from those in holo proteins, are mapped onto the holo atomic models. The mapped color ranges from blue (-2) to red

(2), e.g., the regions with dynamics suppressions exhibited lower values. The color bar represents the dynamics changes. The binding partners and regions disordered in apo proteins are colored green and dark gray, respectively. In the overall view (upper), the Cα atoms of the residues located within 5 Å of the binding partners are indicated by sphere models, and gray colors represents the cryo-EM maps. In EMD-9622 (yeast Ribonuclease P[28], middle), the catalytic RNA is not shown for better viewability. The close-up view of the representative interacting regions is shown in the lower panels in Fig. 4b (dashed rectangles indicate the regions). Stick models indicated the residues intensively discussed in the referred literature. The subunit names used in the literature are denoted as superscripts in the labels. **c**, Allosteric dynamics changes detected with DEFMap. The dynamics suppressions of the regions distal from the ligand-binding site are observed for EMD-20080/EMD-20081 {Arabidopsis defective in meristem silencing 3 (DMS3) - RNA-directed DNA methylation 1(RDM1) in complex with defective in RNA-directed DNA methylation 1 (DRD1) peptide[22]}. The complex is composed of a RDM1 dimer (gray), two DMS3 dimers (dimer 1, magenta; dimer 2, orange), and DRD1 peptide (green), as shown in a middle panel. A DMS3 dimer establishes contacts with one molecule of RDM1 dimer through one of the coiled-coil arms. DRD1 peptide is recognized by RDM1 dimer, coiled-coil arms in DMS3 dimer 1, and a hinge domain in a subunit of DMS3 dimer 2. The DRD1 peptide-binding allosterically induced dynamics suppressions at the RDM1-DMS3 interacting interfaces and the overall regions of the hinge domains in the DMS3 dimer 1. The close-up views of their regions are shown in the left-hand and right-hand side panels, respectively. The color bar indicates the ligand-induced dynamics changes.

Methods

Molecular dynamics simulation

Initial coordinates solved were derived from the PDB (https://www.rcsb.org) and processed by using a Structure Preparation module in the Molecular Operating Environment (MOE). Briefly, loops were modeled for disordered regions whose number of residues was less than seven and the other non-natural N-termini and C-termini were capped with acetyl groups and formyl groups, respectively. Addition of the hydrogen atoms and generation of the topology files were carried out using a pdb2gmx module in the GROMACS[31]. All MD simulations were carried out in periodic boundary conditions (PBC) by using the GROMACS on NVIDIA GeForce GTX 1080 GPU. Amber ff99SB-ILDN force field was used for proteins, nucleotides and ions[32], and TIP3P was used for water molecules[33]. Water molecules were placed around the complex model with an encompassing distance of 10 Å. Counter-ions were added to neutralize the system. Electrostatic interactions were calculated using the particle mesh Ewald (PME) method [34] with a cutoff radius of 10 Å, and a nonbonded cutoff of 10 Å was used for Van der Waals interactions. The P-LINCS algorithm was used to constrain all bond lengths[35]. After energy-minimization of the fully solvated systems, the resulting systems were equilibrated for 100 psec using a constant number of molecules, volume, and temperature condition (NVT) and run for 100 psec employing a constant number of molecules, pressure, and temperature condition (NPT), with the heavy atoms of the macromolecules held in fixed positions. The temperature was maintained at 298 K with velocity re-scaling with a stochastic term[36], and the pressure was maintained at 1 bar with the help of Parrinello-Rahman pressure coupling[37], with temperature and pressure time constants set to 0.1 psec and 2 psec, respectively. Subsequently, twenty-nanosecond production runs were carried out under the NPT condition without positional restraints. The generated trajectories after PBC corrections were aligned using overall Cα atoms, followed by calculations of the RMSF values (Å) for heavy atoms with an rmsf module in the GROMACS. The logarithms of RMSF are used as the dynamics.

Preparation of input data for deep neural networks

Original cryo-EM density maps and the corresponding atomic models with the overall map resolutions less than 4.5 Å, which is relatively high resolution than the average overall resolution of cryo-EM maps deposited in 2019 (5.6 Å), were selected and downloaded from PDB (thirty-four datasets). The training and evaluation datasets were composed of twenty-five and nine macromolecules, respectively (Supplementary Table 1). The maps were rescaled as 1.5 Å/pixel and low-pass filtered to 5, 6, 7, 8, 9 and 10 Å

by using EMAN2.3[30]. Subsequently, the intensities were normalized within each map data and those less than zero were discarded. The grid in the maps were assigned with MD-derived dynamics (logarithmic RMSF) of the nearest atoms in the voxelized coordinate. The resulting maps were sub-voxelized to generate the input density data with the sizes of 10^3 voxels (15^3 Å^3). For training data, we implemented data augmentations by horizontal/vertical rotations with 90, 180 and 270 degrees. Voxelization of atomic models were carried out by utilizing High Throughput Molecular Dynamics (HTMD)[38]. All of the pre-processing was performed using Python.

Construction of deep neural networks

Architecture of the neural network in DEFMap are composed of 3D convolutional blocks and dense blocks. 3D convolutional blocks have three 3D convolutional layers with leaky ReLU activation, max pooling, and dropout. The kernel size for convolution, the pool size of the max pooling, and dropout ratio are set to 4 × 4 × 4, 2 × 2, and 0.2, respectively. The three 3D convolutional layers applied different filter sizes, 64, 128, and 256. Dense blocks have two dense layers of 1024 units with leaky ReLU activation and a dense layer of a unit with identity activation. Hyperparameters was set as epochs = 50, learning rate = 0.00005, and batch size = 128, and utilized early stopping with a patience three to avoid overfitting. All models were trained on NVIDIA Tesla V100 with 16 GB GPU memory. The Keras[39] was employed with Tensorflow[40] backend.

Post-processing and visualization of output from the neural networks

The atomic dynamics values calculated by DEFMap were post-processed for the subsequent validation and analyses as follows; the output values were normalized, followed by averaging for each residue. The residue-specific dynamics values (termed as $\text{Dynamics}^{\text{DEFMap}}$ in the main text) were assigned to atomic models as temperature factors with HTMD[38] and visualized using PyMOL[41] and UCSF Chimera[42]. All of the post-processing was performed using Python.

Software

The following software packages were used: MOE (version: 2016.08; https://www.chemcomp.com/Products.htm) for structure preparation in MD simulation. GROMACS (version:2016.5; http://manual.gromacs.org/documentation/2016/#) for MD simulation. EMAN2.3 (https://blake.bcm.edu/emanwiki/EMAN2) for low-pass filtering and rescaling of cryo-EM map. HTMD (version:1.15.2; https://software.acellera.com/docs/latest/htmd/index.html), Keras (version: 2.2.4; https://keras.io/), Tensorflow (versions: 1.13.1; https://www.tensorflow.org/), and Python (version: 3.6; https://www.python.org/) for development of DEFMap. PyMOL (version:

2.2.0; https://pymol.org/2/) and UCSF Chimera (version: 1.13.1; https://www.cgl.ucsf.edu/chimera/) for dynamics visualizations in DEFMap.

Data availability

All the datasets used in this paper are publicly available from PDB (https://www.rcsb.org/). Detailed descriptions of the dataset are in Supplemental Table 1.

References

1 Boehr, D. D., Nussinov, R. & Wright, P. E. The role of dynamic conformational ensembles in biomolecular recognition. *Nat Chem Biol* **5**, 789-796, doi:10.1038/nchembio.232 (2009).

2 Kohen, A. Role of Dynamics in Enzyme Catalysis: Substantial versus Semantic Controversies. *Accounts of Chemical Research* **48**, 466-473, doi:10.1021/ar500322s (2014).

3 Murata, K. & Wolf, M. Cryo-electron microscopy for structural analysis of dynamic biological macromolecules. *Biochimica et Biophysica Acta (BBA) - General Subjects* **1862**, 324-334, doi:10.1016/j.bbagen.2017.07.020 (2018).

4 Cheng, Y., Grigorieff, N., Penczek, P. A. & Walz, T. A primer to single-particle cryo-electron microscopy. *Cell* **161**, 438-449, doi:10.1016/j.cell.2015.03.050 (2015).

5 Cheng, Y. Single-particle cryo-EM-How did it get here and where will it go. *Science* **361**, 876-880, doi:10.1126/science.aat4346 (2018).

6 Nitta, R., Imasaki, T. & Nitta, E. Recent progress in structural biology: lessons from our research history. *Microscopy (Oxf)*, doi:10.1093/jmicro/dfy022 (2018).

7 Masson, G. R. *et al.* Recommendations for performing, interpreting and reporting hydrogen deuterium exchange mass spectrometry (HDX-MS) experiments. *Nat Methods* **16**, 595-602, doi:10.1038/s41592-019-0459-y (2019).

8 Hollingsworth, S. A. & Dror, R. O. Molecular Dynamics Simulation for All. *Neuron* **99**, 1129-1143, doi:10.1016/j.neuron.2018.08.011 (2018).

9 Frank, J. & Ourmazd, A. Continuous changes in structure mapped by manifold embedding of single-particle data in cryo-EM. *Methods* **100**, 61-67, doi:10.1016/j.ymeth.2016.02.007 (2016).

10 Ji, S., Xu, W., Yang, M. & Yu, K. 3D Convolutional neural networks for human action recognition. *IEEE Transactions on Pattern Analysis and Machine Intelligence* **35**, 221--231, doi:10.1109/TPAMI.2012.59 (2013).

11 Zhirong, W. *et al.* 3D ShapeNets: A deep representation for volumetric shapes. in *IEEE Conference on Computer Vision and Pattern Recognition (CVPR)* 1912-1920 (2015).

12 Maturana, D. & Scherer, S. VoxNet: A 3D Convolutional Neural Network for real-time object recognition. in *2015 IEEE/RSJ International Conference on Intelligent Robots and Systems (IROS)* 922-928 (2015).

13 Girdhar, R., Gkioxari, G., Torresani, L., Paluri, M. & Tran, D. Detect-and-Track: Efficient Pose Estimation in Videos. in *2018 IEEE/CVF Conference on Computer Vision and Pattern Recognition* 350-359 (2018).

14 Grinciunaite, A., Gudi, A., Tasli, E. & den Uyl, M. Human Pose Estimation in Space and Time Using 3D CNN. in *Computer Vision – ECCV 2016 Workshops Lecture Notes in Computer Science* Ch. Chapter 5, 32-39 (2016).

15 Qi, D. *et al.* Automatic Detection of Cerebral Microbleeds From MR Images via 3D Convolutional Neural Networks. *IEEE Trans Med Imaging* **35**, 1182-1195, doi:10.1109/TMI.2016.2528129 (2016).

16 Kamnitsas, K. *et al.* Efficient multi-scale 3D CNN with fully connected CRF for accurate brain lesion segmentation. *Medical Image Analysis* **36**, 61--78, doi:10.1016/j.media.2016.10.004 (2017).

17 Chen, H., Dou, Q., Yu, L., Qin, J. & Heng, P.-A. VoxResNet: Deep voxelwise residual networks for brain segmentation from 3D MR images. *NeuroImage* **170**, 446-455, doi:10.1016/j.neuroimage.2017.04.041 (2018).

18 Xu, K., Wang, Z., Shi, J., Li, H. & Zhang, Q. C. A2-Net: Molecular Structure Estimation from Cryo-EM Density Volumes. *Proceedings of the AAAI Conference on Artificial Intelligence* **33**, 1230-1237 (2019).

19 Mostosi, P., Schindelin, H., Kollmannsberger, P. & Thorn, A. Automated interpretation of Cryo-EM density maps with convolutional neural networks. *bioRxiv*, 644476, doi:10.1101/644476 (2019).

20 Avramov, T. K. *et al.* Deep learning for validating and estimating resolution of cryo-electron microscopy density maps. *Molecules* **24**, 1181, doi:10.3390/molecules24061181 (2019).

21 Maddhuri Venkata Subramaniya, S. R., Terashi, G. & Kihara, D. Protein secondary structure detection in intermediate-resolution cryo-EM maps using deep learning. *Nat Methods* **16**, 911-917, doi:10.1038/s41592-019-0500-1 (2019).

22 Tagari, M., Newman, R., Chagoyen, M., Carazo, J. M. & Henrick, K. New electron microscopy database and deposition system. *Trends Biochem Sci* **27**, 589, doi:10.1016/s0968-0004(02)02176-x (2002).

23 Berman, H. M. The Protein Data Bank. *Nucleic Acids Research* **28**, 235-242, doi:10.1093/nar/28.1.235 (2000).

24 Zhang, W., Lukoyanova, N., Miah, S., Lucas, J. & Vaughan, C. K. Insights into Centromere DNA Bending Revealed by the Cryo-EM Structure of the Core Centromere Binding Factor 3 with Ndc10. *Cell Reports* **24**, 744-754, doi:10.1016/j.celrep.2018.06.068 (2018).

25 Sun, Y. *et al.* Molecular basis for the recognition of the human AAUAAA polyadenylation signal. *Proceedings of the National Academy of Sciences* **115**, E1419-E1428, doi:10.1073/pnas.1718723115 (2018).

26 Cash, J. N. *et al.* Cryo–electron microscopy structure and analysis of the P-Rex1–Gβγ signaling scaffold. *Science Advances* **5**, doi:10.1126/sciadv.aax8855 (2019).

27 Wongpalee, S. P. *et al.* CryoEM structures of Arabidopsis DDR complexes involved in RNA-directed DNA methylation. *Nature Communications* **10**, doi:10.1038/s41467-019-11759-9 (2019).

28 Lan, P. *et al.* Structural insight into precursor tRNA processing by yeast ribonuclease P. *Science* **362**, doi:10.1126/science.aat6678 (2018).

29 Abascal-Palacios, G., Ramsay, E. P., Beuron, F., Morris, E. & Vannini, A. Structural basis of RNA polymerase III transcription initiation. *Nature* **553**, 301-306, doi:10.1038/nature25441 (2018).

30 Tang, G. *et al.* EMAN2: An extensible image processing suite for electron microscopy. *Journal of Structural Biology* **157**, 38-46, doi:https://doi.org/10.1016/j.jsb.2006.05.009 (2007).

31 Abraham, M. J. *et al.* GROMACS: High performance molecular simulations through multi-level parallelism from laptops to supercomputers. *SoftwareX* **1-2**, 19-25, doi:10.1016/j.softx.2015.06.001 (2015).

32 Lindorff-Larsen, K. *et al.* Improved side-chain torsion potentials for the Amber ff99SB protein force field. *Proteins: Structure, Function, and Bioinformatics*, NA-NA, doi:10.1002/prot.22711 (2010).

33 Jorgensen, W. L. & Thomas, L. L. Perspective on Free-Energy Perturbation Calculations for Chemical Equilibria. *J Chem Theory Comput* **4**, 869-876, doi:10.1021/ct800011m (2008).

34 Darden, T., York, D. & Pedersen, L. Particle Mesh Ewald - an N.Log(N) Method for Ewald Sums in Large Systems. *J Chem Phys* **98**, 10089-10092, doi:Doi 10.1063/1.464397 (1993).

35 Hess, B. P-LINCS: A parallel linear constraint solver for molecular simulation. *J Chem Theory Comput* **4**, 116-122, doi:10.1021/ct700200b (2008).

36 Bussi, G., Donadio, D. & Parrinello, M. Canonical sampling through velocity rescaling. *The Journal of Chemical Physics* **126**, doi:10.1063/1.2408420 (2007).

37 Parrinello, M. & Rahman, A. Polymorphic transitions in single crystals: A new molecular dynamics method. *Journal of Applied Physics* **52**, 7182-7190, doi:10.1063/1.328693 (1981).

38 Doerr, S., Harvey, M. J., Noe, F. & De Fabritiis, G. HTMD: High-Throughput Molecular Dynamics for Molecular Discovery. *J Chem Theory Comput* **12**, 1845-1852, doi:10.1021/acs.jctc.6b00049 (2016).

39 Chollet, F. Keras. https://keras.io (2015).

40 Abadi, M. *et al.* TensorFlow: A system for large-scale machine learning. 265-283 (2016).

41 Schrdinger, L. L. C. The PyMOL Molecular Graphics System. (2015).

42 Pettersen, E. F. *et al.* UCSF Chimera—A visualization system for exploratory research and analysis. *Journal of Computational Chemistry* **25**, 1605-1612, doi:10.1002/jcc.20084 (2004).